Int. J. Heat Mass Transfer. Vol. 27, No. 2, pp. 253 262, 1984
Printed in Great Britain

0017 9310/84 $3.00 + 0.00
Pergamon Press Ltd.

THE PREDICTION OF TURBULENT FLOW AND HEAT TRANSFER IN A NARROW ISOSCELES TRIANGULAR DUCT

C. W. RAPLEY
Department of Mechanical Engineering, Sunderland Polytechnic, Edinburgh Building, Chester Road, Sunderland SR1 3SD, U.K.

and

A. D. GOSMAN
Department of Mechanical Engineering, Imperial College of Science and Technology, London, U.K.

(*Received* 27 *March* 1983 *and in revised form* 2 *June* 1983)

Abstract— Predictions are described of fully developed turbulent flow and heat transfer in a narrow isosceles triangular duct obtained by means of a computer model in which the Reynolds stresses are calculated from algebraic forms of their transport equations, first derived for square duct calculations. The governing equations are formulated in an orthogonal curvilinear coordinate frame which is fitted to the shape of the duct cross-section, and are solved by an efficient finite volume method. The solutions presented show that, for the conditions of the small apex angle duct examined, the local and overall heat transfer is relatively unaffected by secondary flow, whilst being quite sensitive to the imposed temperature boundary conditions. The predictions compare satisfactorily with the experiments and were found also to be useful in interpreting them.

NOMENCLATURE

A_i	finite volume coefficients
ASTM	algebraic stress transport model
$C_{\varepsilon 1}, C_{\varepsilon 2}$	constants in equation (18): $C_{\varepsilon 1} = 1.55$, $C_{\varepsilon 2} = 2.0$
$C_{\phi 1}, C_{\phi 2}$	coefficients in the ASTM: $C_{\phi 1} = 2.78$, $C_{\phi 2} = 0.358$
D_e	equivalent (hydraulic) diameter
f	friction factor ($\bar{\tau}_s/0.5\rho\bar{U}_3^2$)
h_i	metric coefficients
k	turbulence kinetic energy
Nu	Nusselt number
p	pressure
P	production rate of k
Pr	laminar Prandtl number
q	local surface heat flux
$\bar{q}$	mean surface heat flux
r_i	local radii of curvature
Re	Reynolds number ($\rho U_3 D_e/\mu$)
t_{ij}	turbulent stress tensor
T	temperature
T_b	bulk fluid temperature
T_w	local wall temperature
$\bar{T}_w$	mean wall temperature
u_i	fluctuating velocity component
$\overline{u_i u_j}$	Reynolds kinematic stresses
$\overline{u_i\theta}$	turbulent heat fluxes
U_i	local velocity component
$\bar{U}_i$	average velocity component
U_3^*	friction velocity
x_i	Cartesian coordinates.

Greek symbols

ε	dissipation rate of k
θ	fluctuating temperature
μ	laminar viscosity
μ_t	turbulent viscosity
ξ_i	general orthogonal coordinates
ρ	fluid density
σ_ϕ	turbulent Prandtl number: $\sigma_k = 1.0$, $\sigma_\varepsilon = 1.2$, $\sigma_t = 0.9$
τ_{ij}	viscous stress tensor
τ_s	local wall shear stress
$\bar{\tau}_s$	average wall shear stress
Γ	molecular diffusivity of heat
Γ_t	turbulent diffusivity of heat
γ_{ij}	total stress tensor
ϕ	any main variable.

INTRODUCTION

THE DESIGN of effective compact heat exchanger systems depends critically on knowledge of the local mean flow and heat transfer characteristics of non-circular passages. Triangular passages with small apex angles are one of the many possible shapes which could be, and are, used to achieve high compactness. However, when the flow is turbulent, very little information appears to be available for local mean flow and heat transfer distributions in such passages, as shown in the summary given in ref. [1]. This is perhaps because the acute-angled internal corners pose obvious measurement difficulties, particularly when the angle is less than 30°. Some turbulent flow measurements of fully developed friction factors have been reported for isosceles triangular ducts with apex angles of between 4° and 24.8° [2–4]. Eckert and Irvine [2] also reported local axial velocity data for apex angles of 11.7° and 24.8°. Their 11.7° angled duct was later extended in length from 80 to 167 equivalent diameters, apparently to achieve fully developed flow, and used for turbulence

measurements which were reported by Cremers and Eckert [5]. No further local axial velocity distributions appear to have been published for this extended duct.

The equilateral triangular duct experiments of Aly *et al.* [6] appear to be the only other detailed measurements reported for triangular ducts. Although the corner angles are larger than those discussed above, the results are of interest since they include measurements of the turbulence driven secondary flows which exist in the cross-plane of all straight non-circular passages and are in the form, in this instance, shown in Fig. 1. This circulation confirmed the earlier deductions of Nikuradse [7] from his measured axial velocity contours which bulged into the corners indicating that there is convection from the duct core towards the corners. The measured axial velocity and turbulence kinetic energy contours of Aly *et al.* [6] were found also to bulge, the latter even more markedly than the former, into the corners. As seen from Fig. 1, from symmetry and continuity requirements the secondary flow recirculates from the corner back to the core through the regions adjacent to the duct wall and the normal plane bisecting the wall giving six symmetrical counter rotating circulations in the duct cross-plane. Indirect evidence of the presence of secondary flows in the 11.7° apex angle duct of ref. [2] was apparent in the axial velocity profiles which showed larger velocities near the corners than in the centre-plane. The velocity profiles also showed distortions (rapid changes in gradient) in the apex corner region (see Fig. 5) although the authors could find no explanation for these.

Local and overall heat transfer measurements have been made by Eckert and Irvine [8] in a narrow isosceles triangular duct with an apex angle of 11.5° and stainless steel walls which were heated directly with an alternating electrical current. The mean Nusselt numbers, based on hydraulic diameter, were found to be only 60% of the circular tube values and the measured local temperatures on the long wall ranged from 0.2 (at the duct base) to 2.4 (at the apex) times their mean level. The constant wall heat flux condition expected with direct heating was found not to have occurred with measurements indicating wall heat fluxes in the base region many times those in the apex region on the long wall. The authors concluded, in a written discussion of their work, that the actual boundary conditions were about mid-way between constant wall heat flux and constant wall temperature.

Turning now to theoretical studies, none that include secondary flow have been reported for fully developed turbulent flow in acute angled triangles, but some investigations have been published for other passage shapes. These include square ducts [9, 10], rod bundles [11–13] and an equilateral triangular duct [6]. All of these employed numerical finite-difference procedures and all except refs. [10, 13] used the method of Gosman *et al.* [14] to solve the vorticity/stream function formulation of the equations of motion. The cross-plane turbulent stresses were calculated with simplified algebraic forms of the Reynolds stress transport equations (ASTM) first proposed by Launder and Ying [9] and which requires values of turbulence kinetic energy k and its dissipation rate ε. All methods solved a modelled differential transport equation for k and calculated ε from turbulent length scales which were prescribed either from experiment or from the Buleev [15] geometric formula with the exception of ref. [13] where a differential transport equation for ε was solved. The methods of Naot *et al.* [10] and Bartzis and Todreas [13] solved the velocity–pressure forms of the momentum and continuity equations with the former employing differential transport equations for the required stresses and the latter using both the ASTM and the algebraic empirical relations suggested by Bobkov *et al.* [16].

In order to obtain reasonable convergence in the foregoing studies it was found necessary in most cases to simplify the stress derivatives responsible for vorticity generation by either omitting the cross-plane shear stresses or prescribing the direction of the recirculating secondary flow by imposing an immutable sign.

The square and triangular duct predictions all showed the expected secondary flow circulations and were in reasonable general agreement with experiment with the convective transport effects of secondary motions clearly evident. The rod bundle calculations were in less agreement, with predicted secondary flow patterns of from one to three separate circulations being variously obtained in a symmetry sub-channel of an infinite triangular array. Measurements, however, indicate that a single circulation is the most likely secondary flow in closely spaced rod bundle symmetry sub-channels [17]. Comparisons between calculations with and without secondary flows in all of these cases indicated significant secondary flow effects in the local mean flow and turbulence kinetic energy distribution, particularly in the latter.

Little attention appears to have been paid to the simultaneous prediction of fully developed local turbulent flow and heat transfer in non-circular passages with inclusion of secondary flow modelling. A few studies are reported for square ducts [9, 18], an elliptical duct [19] and rod bundles [19, 20]. In all cases the turbulent heat fluxes in the thermal energy balance were calculated from Fourier-law expressions containing isotropic eddy diffusivities based on the assumption of constant turbulent Prandtl number. Secondary flow was generally found to have a significant influence in

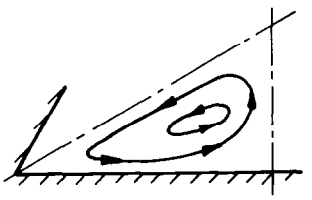

FIG. 1. Measured secondary flow pattern in an equilateral triangular duct.

making the peripheral distribution of local heat transfer more uniform than it would otherwise be. As a consequence, and in contrast to laminar flow, turbulent heat transfer was seen to be relatively insensitive to the applied boundary conditions.

The present work is based on a general finite volume method developed for the prediction of fully developed flow and heat transfer in arbitrary shaped passages [19, 21, 22]. The equations of motion are solved in general curvilinear orthogonal coordinate forms with velocities and pressure as the dependent variables. The turbulent stresses are calculated from the ASTM of Launder and Ying [9] in the form proposed by Gessner and Emery [23] which provides explicit relations between stresses and strains for the full stress tensor. This ASTM is employed together with the k–ε transport equations to avoid the need for empirical specification of the turbulence length scale distributions.

The case of an acute apex angled isosceles triangular duct considered here represents a severe test of calculation methods of this kind since the velocities and turbulence properties change rapidly across the narrow duct and exhibit asymmetries caused by the small and large angled internal corners. A further unique feature of this flow is the significant damping effect of the walls on turbulence in the acute angled apex corner.

THE GOVERNING EQUATIONS

Mean motion and heat transfer

In the detailed development of the partial differential equations representing the flow and heat transfer in ref. [22] they are first expressed in Cartesian tensor notation, with U_i, p and T standing for mean velocity, pressure and temperature, respectively thus

$$\partial(\rho U_i U_j)/\partial x_i = -\partial p/\partial x_i + \partial(\gamma_{ij})/\partial x_i, \tag{1}$$

$$\partial(\rho U_i)/\partial x_i = 0, \tag{2}$$

$$\partial(\rho U_i T)/\partial x_i = \partial(\Gamma \partial T/\partial x_i - \overline{u_i\theta})/\partial x_i. \tag{3}$$

In the above the stress tensor γ_{ij} is the sum of the viscous stress tensor τ_{ij}, given by the Newtonian law

$$\tau_{ij} = \mu(\partial U_i/\partial x_j + \partial U_j/\partial x_i), \tag{4}$$

and the Reynolds turbulent stresses t_{ij} which are defined in terms of the fluctuating velocities u_i by

$$t_{ij} = -\overline{\rho u_i u_j}, \tag{5}$$

where the overbar indicates time averaging. Γ stands for the molecular diffusivity of heat whilst $\overline{u_i\theta}$ are the turbulent heat fluxes, θ being the fluctuating temperature.

For the present application the above equations are recast into a coordinate form which is general orthogonal in the duct cross-section and rectilinear in the axial direction, with the aid of the transformation relations derived by Pope [24]. When the appropriate simplifications are invoked for fully developed flow and heat transfer in straight passages (i.e. $\partial/\partial\xi_3 = 0$ for all variables apart from pressure and temperature) the equations become:

direction 1 (cross-plane)

$$\begin{aligned}&\partial(h_2\rho U_1U_1)/\partial\xi_1 + \partial(h_1\rho U_1U_2)/\partial\xi_2\\ &= -h_2\,\partial p/\partial\xi_1 - \partial(h_2\gamma_{11})/\partial\xi_1\\ &\quad -\partial(h_1\gamma_{12})/\partial\xi_2 - h_1h_2(\rho U_1U_2+\gamma_{12})/r_1\\ &\quad +h_1h_2(\rho U_1U_2+\gamma_{22})/r_2;\end{aligned} \tag{6}$$

direction 2 (cross-plane)

$$\begin{aligned}&\partial(h_2\rho U_1U_2)/\partial\xi_1 + \partial(h_1\rho U_2U_2)/\partial\xi_2\\ &= -h_1\,\partial p/\partial\xi_2 - \partial(h_2\gamma_{12})/\partial\xi_1\\ &\quad -\partial(h_1\gamma_{22})/\partial\xi_2 + h_1h_2(\rho U_1U_1+\gamma_{11})/r_1\\ &\quad -h_1h_2(\rho U_1U_2+\gamma_{12})/r_2;\end{aligned} \tag{7}$$

direction 3 (axial)

$$\begin{aligned}&\partial(h_2\rho U_1U_3)/\partial\xi_1 + \partial(h_1\rho U_2U_3)/\partial\xi_2\\ &= -h_1h_2\,\mathrm{d}p/\mathrm{d}\xi_3 - \partial(h_2\gamma_{13})/\partial\xi_1\\ &\quad -\partial(h_1\gamma_{23})/\partial\xi_2;\end{aligned} \tag{8}$$

energy

$$\begin{aligned}&\partial(h_2\rho U_1T)/\partial\xi_1 + \partial(h_1\rho U_2T)/\partial\xi_2\\ &+\mathrm{d}(h_1h_2\rho U_3T)/\mathrm{d}\xi_3 = \partial(\Gamma h_2\,\partial T/h_1\,\partial\xi_1)/\partial\xi_1\\ &+\partial(\Gamma h_1\,\partial T/h_2\,\partial\xi_2)/\partial\xi_2\\ &-\partial(h_2\overline{u_1\theta})/\partial\xi_1 - \partial(h_1\overline{u_2\theta})/\partial\xi_2.\end{aligned} \tag{9}$$

Here ξ_1 and ξ_2 are the orthogonal coordinates, ξ_3 is the axial coordinate and h_1, h_2 and unity are the respective metrics. The cross-planar velocity components U_1 and U_2 are aligned with ξ_1 and ξ_2, respectively, while U_3 is the axial component.

Turbulent stress and heat flux models

The Reynolds stresses are here calculated from the following simplified algebraic stress model (ASTM) versions of the Reynolds stress transport equations as proposed by Launder and Ying [9] and Gessner and Emery [23].

$$\overline{u_3^2} = C_1k, \tag{10}$$

$$\overline{u_2^2} = C_3k - C_2C_4(k^3/\varepsilon^2)(\partial U_3/h_2\,\partial\xi_2)^2, \tag{11}$$

$$\overline{u_1^2} = C_3k - C_2C_4(k^3/\varepsilon^2)(\partial U_3/h_1\,\partial\xi_1)^2, \tag{12}$$

$$\overline{u_1u_2} = -C_2C_4(k^3/\varepsilon^2)(\partial U_3/h_1\,\partial\xi_1)(\partial U_3/h_2\,\partial\xi_2), \tag{13}$$

$$\overline{u_1u_3} = -C_4(k^2/\varepsilon)\,\partial U_3/h_1\,\partial\xi_1, \tag{14}$$

$$\overline{u_2u_3} = -C_4(k^2/\varepsilon)\,\partial U_3/h_2\,\partial\xi_2. \tag{15}$$

Here C_1, C_2, C_3 and C_4 are constants linked together by the relations given in the Appendix.

The axial plane shear stresses $\rho\overline{u_1u_3}$ and $\rho\overline{u_2u_3}$ are seen from equations (14) and (15) to be represented by a

Newtonian type of relation with a turbulent viscosity μ_t given by

$$\mu_t = C_4 \rho k^2/\varepsilon, \tag{16}$$

where k is the kinetic energy of turbulence and ε is its dissipation rate. In contrast, the cross-plane stresses, which are responsible for secondary motions, are given by equations (11)–(13) and are seen to depend on strain rates in planes orthogonal to the cross-plane.

The quantities k and ε required in the ASTM are obtained from the appropriate form of the well known k–ε turbulence model [25] which, for the present circumstances gives rise to the following transport equations for these variables

$$\begin{aligned}&\partial(h_2\rho U_1 k)/\partial\xi_1 + \partial(h_1\rho U_2 k)/\partial\xi_2 \\ &= h_1h_2P - h_1h_2\rho\varepsilon + \partial(h_2(\mu_t/\sigma_k)\,\partial k/h_1\,\partial\xi_1)/\partial\xi_1 \\ &\quad + \partial(h_1(\mu_t/\sigma_k)\,\partial k/h_2\,\partial\xi_2)/\partial\xi_2,\end{aligned} \tag{17}$$

$$\begin{aligned}&\partial(h_2\rho U_1\varepsilon)/\partial\xi_1 + \partial(h_1\rho U_2\varepsilon)/\partial\xi_2 \\ &= h_1h_2C_{\varepsilon1}\varepsilon P/k - h_1h_2C_{\varepsilon2}\rho\varepsilon^2/k \\ &\quad + \partial(h_2(\mu_t/\sigma_\varepsilon)\,\partial\varepsilon/h_1\,\partial\xi_1)/\partial\xi_1 \\ &\quad + \partial(h_1(\mu_t/\sigma_\varepsilon)\,\partial\varepsilon/h_2\,\partial\xi_2)/\partial\xi_2,\end{aligned} \tag{18}$$

where σ_k and σ_ε are the turbulent Prandtl numbers for k and ε, respectively, and P is the production rate of turbulence kinetic energy, calculated from

$$P = -\rho\overline{u_1u_3}\,\partial U_3/h_1\,\partial\xi_1 - \rho\overline{u_2u_3}\,\partial U_3/h_2\,\partial\xi_2. \tag{19}$$

The turbulent heat fluxes are represented by a single gradient diffusion model incorporating an isotropic turbulent diffusivity of heat Γ_t i.e.

$$\begin{aligned}-\overline{u_1\theta} &= \Gamma_t\,\partial T/h_1\,\partial\xi_1, \\ -\overline{u_2\theta} &= \Gamma_t\,\partial T/h_2\,\partial\xi_2.\end{aligned} \tag{20}$$

Here Γ_t is taken to be equal to the ratio μ_t/σ_t where σ_t, the turbulent Prandtl number for heat, is assumed to have a constant value.

Conventionally, wall functions are used to bridge between the boundary surfaces and the interior solution. The well-known logarithmic 'law of the wall' is employed as the velocity function and similar universal type relations arising from the equilibrium Couette flow assumption are employed for the turbulence quantities and temperature [22, 25, 26]. The matching to the interior solution was made typically at y^+ values in the range 10–50, the lower value being in the apex corner where the flow was close to laminar.

The values of the various empirical constants appearing in the foregoing equations are taken from previous work [6, 9, 19, 22, 26] and are given in the nomenclature.

THE NUMERICAL SOLUTION METHOD

The finite-difference equations

The transport equations for U_1, U_2, U_3, T, k and ε are discretized by the finite volume method on the curvilinear mesh arrangement of Fig. 2 on which the grid lines and main finite volume boundaries are shown as solid and dashed lines, respectively. The dependent variables are, with two exceptions, calculated at the grid intersections or nodes; the exceptions are the cross-planar velocities U_1 and U_2 which are laterally displaced so as to lie normal to the finite volume surfaces.

The convection and diffusion terms in the differential equations are discretized with a conventional hybrid differencing scheme [27] which is essentially central differencing with provision to switch to upwind when convection dominates. Central differencing is employed with the remaining (source/sink) terms which are linearized where appropriate so as to avoid generating negative values of positive definite quantities such as U_3, k and ε in the course of calculation. The cross-planar momentum equations are discretized with respect to their own finite volumes, displaced so as to be centred about the U_1 and U_2 velocity locations. The resulting finite volume equations are of the general form

$$(\Sigma A_i + S_1)\phi p = \Sigma A_i\phi_i + S_2, \tag{21}$$

where ϕ stands for any of the dependent variables U_1, U_2, U_3, k, ε and T, the A_i's are non-negative coefficients expressing the combined influence of convection and diffusion, the S's are non-negative source/sink coefficients and Σ denotes the summation about the four nodes N, S, E, W adjoining the typical node P in Fig. 2. The resulting coefficient matrix is therefore pentadiagonal and diagonally dominant.

The finite volume equations are solved iteratively in a sequential fashion, adjusting each variable in turn while holding the others frozen, in an outer iteration sequence which is repeated until convergence. Within this sequence the momentum–continuity linkage connecting U_1, U_2 and p is handled via the 'SIMPLE' [27] algorithm, wherein pressure is obtained from its own elliptic equation, derived by taking the divergence of simplified forms of the momentum equations. The solution of the pressure and other equation sets is achieved by inner iteration sequences, using an alternating direction line iteration procedure.

The strong non-linearities and coupling of the

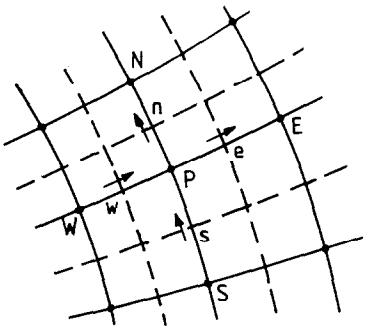

FIG. 2. Orthogonal curvilinear grid.

equations necessitated the development of various *ad hoc* measures to procure convergence of the above procedure. These comprise a special starting procedure, in which the U_1 and U_2 calculations are initially suppressed until the other fields are nearly converged; gradual introduction thereafter of the cross-planar velocity calculation, with strong (50% or more) underrelation; and block adjustment of axial velocities at each iteration, in a manner which ensures overall axial momentum conservation. The convergence requirement is for the sum of the absolute residual sources over the whole field to be less than 10^{-3} times the reference quantities based on the overall mass and momentum flows.

Extensive accuracy tests were performed on the numerical procedure, focusing attention particularly on the effects of the curvilinear mesh on the solution [22]. These included calculations for laminar flow and comparisons with analytical solutions, as in Fig. 3 which relates to flow in an isosceles triangular duct with an apex angle of 11.7° and shows good agreement. Additional confidence was gained from turbulent flow tests which demonstrated that the procedure could produce the expected symmetrical secondary flow patterns in an equilateral triangular duct [21]. From these tests it was also established that meshes with around 250 interior nodes usually produced solutions that were substantially grid independent [22].

PREDICTIONS FOR TURBULENT FLOW

Hydrodynamics

Calculations for an isosceles triangular half duct with a total apex angle of 11.7° will now be shown and compared with the measurements of Eckert and Irvine [2] and Cremers and Eckert [5]. Where appropriate, calculations with secondary flow suppressed are also included to highlight their effect.

The predicted secondary flows are shown in Fig. 4 in the form of projections of the velocity vectors onto the cross-sectional plane and an accompanying sketch indicates the implied recirculation cells. Although there are no measurements available for comparison, the predictions appear plausible with three counter-rotating circulations disposed about the corner bisecting planes as has also been found from measurements in an equilateral triangular duct (see Fig. 1). However, in this case the recirculation cells are not identical, as in the equilateral triangular duct case, but are each a different size and shape as may be expected with the acute angled geometry, namely: the circulation into the long apex corner is elongated and the largest whilst that in the short base corner region is the smallest. These flows also fit the general pattern observed in other non-circular ducts, with flow from the core into the corners along the general direction of corner bisectors, returning to the core along a path adjacent to the wall and planes normal to the wall [22].

Axial velocity profiles along the duct centre plane for two Reynolds numbers are compared with the pitot tube measurements of ref. [2] in Fig. 5. The differences between prediction and experiment may be accounted for in part by incomplete development and also by possible suppression of turbulence in the duct apex corner. The co-existence of laminar and turbulent flow in narrow triangular ducts is a well-known phenomenon [2, 28, 29] and the higher measured axial velocities in the apex corner could be due to lower drag associated with laminar flow. It is also of interest to note that a weak dependence of U_3 on Reynolds number is

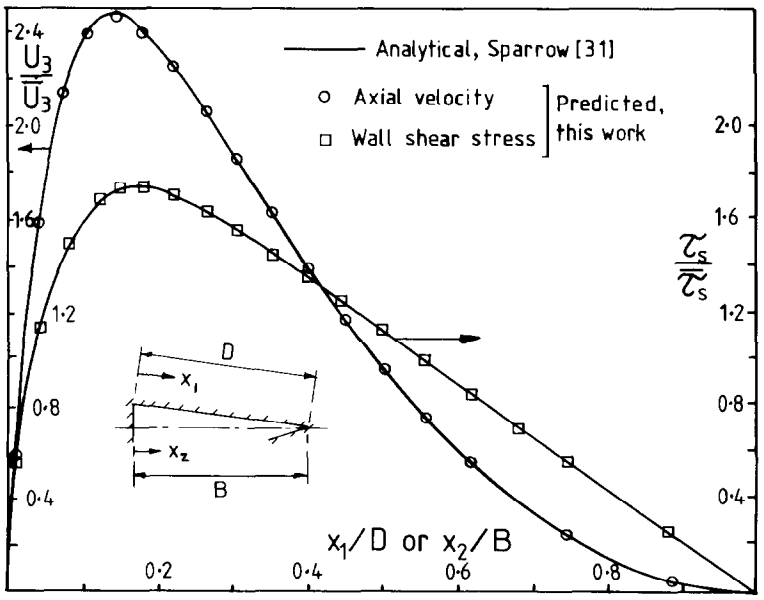

FIG. 3. Laminar centre-plane axial velocity and wall shear stress.

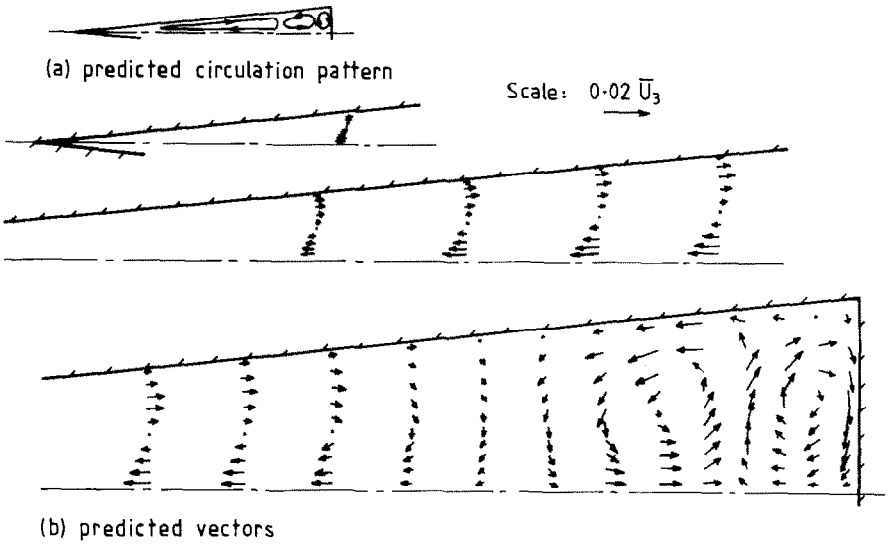

FIG. 4. Predicted secondary velocity vectors and circulation pattern, $Re = 10900$.

apparent in the predictions but not in the measurements.

It should be noted here that although the stress representation in the present method is valid in the limiting cases of fully laminar and fully turbulent flow, it may well be in error in the transitional regime.

Figure 6 compares the local wall shear stress measurements of Cremers and Eckert [5] with the present predictions for both laminar and turbulent flow cases. The agreement is moderate and as may be expected, both experiment and prediction are close to the laminar case in the narrow corner.

Predictions of turbulence kinetic energy and normal stresses are plotted along with the measurements of Cremers and Eckert [5] in Fig. 7. The steep gradients of these quantities near the base wall are well predicted as is the more gradual decay of turbulence, due to the damping effect of the walls, into the acute corner.

The calculated friction factor characteristics for this duct are presented in Fig. 8, together with the measurements and a curve representing the well-known Blasius formula for circular tubes, here evaluated using the hydraulic diameter. The present method has slightly underpredicted the measurements, which may be due in part to lack of full flow development in the latter, and also in part to inadequacies in stress modelling in the calculations, particularly with regard to 'laminarization' effects in the flow. The Blasius equation substantially overestimates f, thus indicating the inadequacy of the hydraulic diameter concept for this duct.

A feature of the calculations which, from previous work in non-circular passages [22], appears to be largely missing from the present predictions, is distortions of the various profiles due to secondary flow. Since, from previous measurements and calculation in other non-circular passages [6, 11, 22], turbulence kinetic energy would be expected to be quite

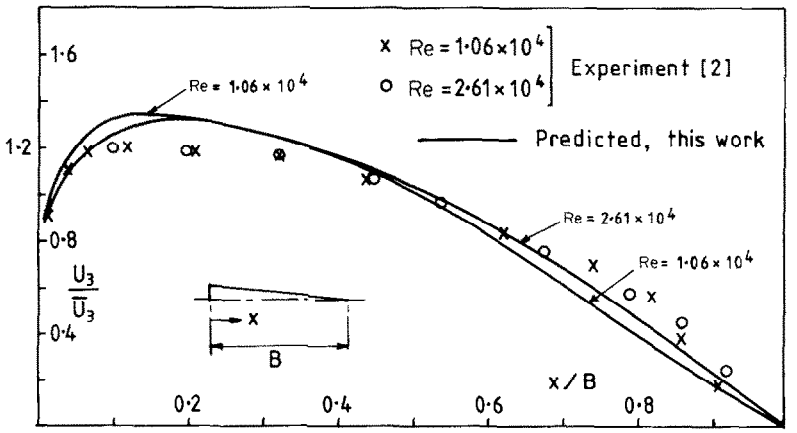

FIG. 5. Centre-plane axial velocity profiles.

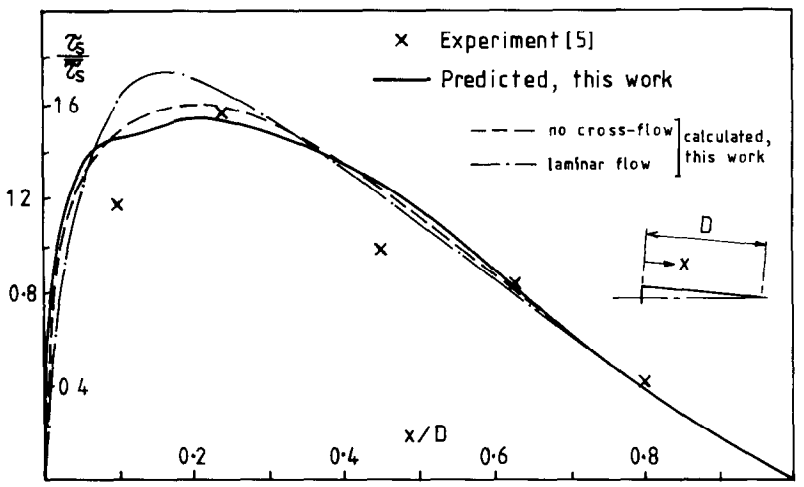

FIG. 6. Wall shear stress profiles, $Re = 10900$.

sensitive to secondary motions, Fig. 7 implies a generally small effect in this duct. This is confirmed by the wall shear stress profiles in Fig. 6.

Heat transfer

The heat transfer calculations are compared with the measurements of Eckert and Irvine [8] for airflow in an isosceles triangular duct with electrically heated walls and an apex angle of 11.5°. The nominal experimental boundary condition is one of constant heat flux (hereafter referred to as 'constant Q_w') but, as mentioned earlier, the measurements showed a significant peripheral variation in both temperature and heat flux on the long wall (only one temperature point is shown on the short wall) and the authors concluded that the actual boundary conditions lay somewhere between constant Q_w and the combination of constant peripheral temperature and constant heat input per unit duct length, here denoted as 'constant T_w'. This is supported by the present calculations which show Figs. 9 and 10, the measured heat flux variation on the long wall to be less than that predicted for the constant T_w case and the measured temperature variation to be also less than that predicted for the constant Q_w case. Further calculations were therefore made with the measured distributions imposed as boundary conditions on the long walls and the intended constant heat flux condition, here taken as the mean heat flux, set along the short wall. The results from these calculations are also plotted in Figs. 9 and 10, and suggest that the measured temperature profile does not correspond to the measured heat flux profile, although this discrepancy could of course alternatively be due to inadequacies in the calculations, perhaps with turbulence modelling or wall function. None of the predicted profiles agree particularly well with the measurements and the response in the calculations, to the alternative boundary conditions derived from the measurements, is seen to be much less than the discrepancies with the data. If, on the other hand, the error lies in the measurements, then it is most likely to be in the determination of wall heat flux, which was not measured directly but inferred from local temperature measurements.

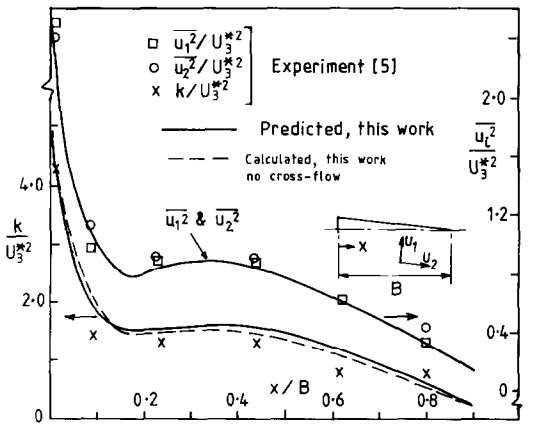

FIG. 7. Centre-plane turbulence kinetic energy and normal stress profiles, $Re = 10900$.

Further evidence to support the latter conclusion can be found in the overall heat transfer comparison in Fig. 11. The measured mean Nusselt numbers are seen to lie, as expected from the above discussion, between the predictions for the constant Q_w and constant T_w boundary conditions. However, the prediction based on measured heat flux lies well below the data, whereas that based on the measured wall temperature distribution is in reasonable accord. Also shown in Fig. 11 is a curve based on the circular tube heat transfer correlation of Kays [30] for gases. This lies some 50% above the data, suggesting that the hydraulic diameter is also not applicable for heat transfer prediction in this duct. The reduced surface heat transfer is most likely due to the damped turbulence effects in the narrow corner region.

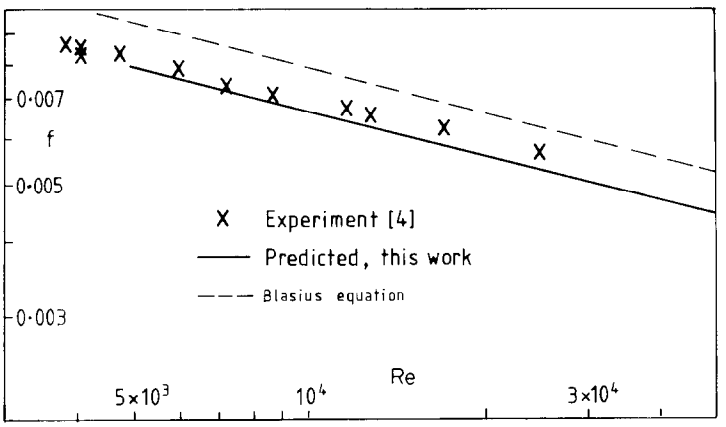

FIG. 8. Friction factor characteristics.

It is noteworthy that, in contrast to previous turbulent heat transfer measurements and calculations in square and elliptical ducts and rod bundles, the thermal boundary conditions here have a significant effect on local and overall heat transfer. This is most likely due to the combined effects of duct geometry and laminarization which have caused relatively large peripheral variations of wall heat flux and temperature which in this case have not been significantly effected by secondary flow which would normally have been expected to reduce these variations. This latter observation is consistent with the small secondary flow effects noted previously in the discussion of the flow predictions.

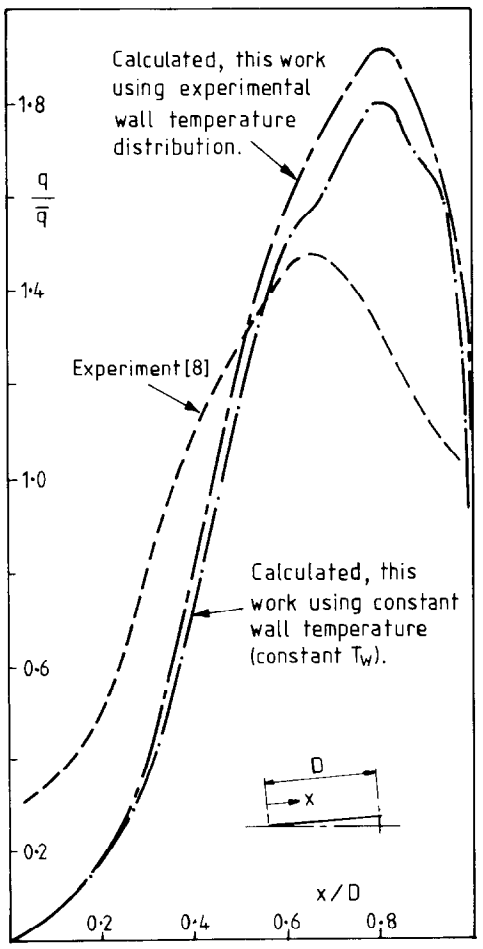

FIG. 9. Peripheral wall heat flux, $Re = 15000$ and $Pr = 0.7$.

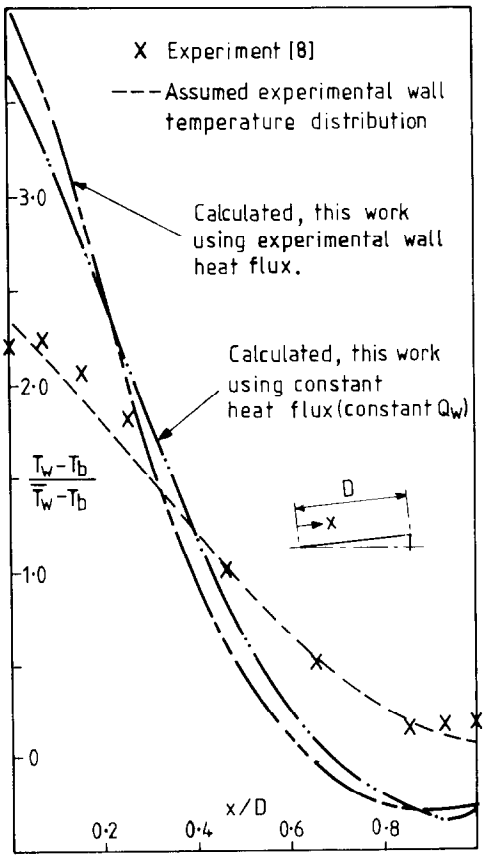

FIG. 10. Peripheral wall temperature, $Re = 15000$ and $Pr = 0.7$.

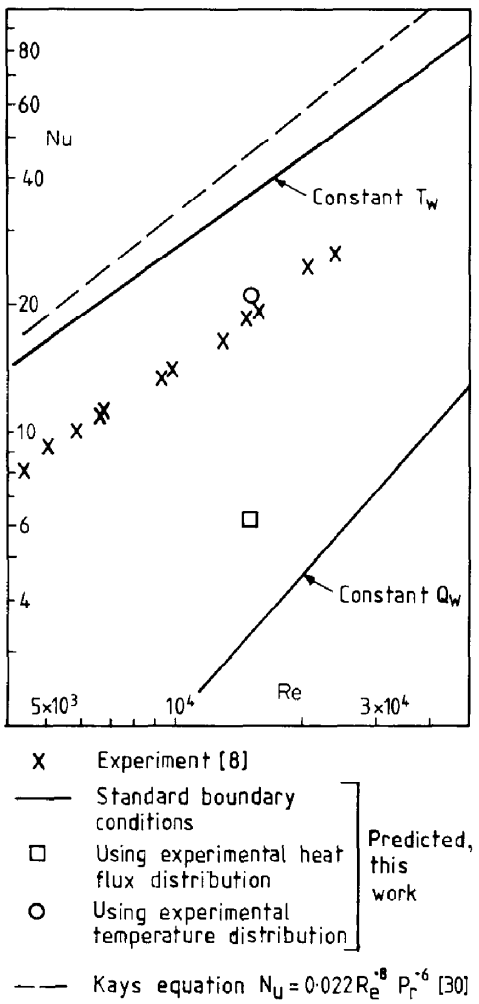

FIG. 11. Mean Nusselt numbers, $Pr = 0.7$.

CONCLUSIONS

Turbulent flow and heat transfer calculations have been made for a narrow isosceles triangular duct. The turbulent stress model used has enabled plausible predictions of the secondary flows, although the calculations made with the latter suppressed indicate that these have only a minor influence on local mean flow and heat transfer in this type of duct. The stress model has also produced satisfactory predictions of the turbulence kinetic energy and normal stress profiles with the damping effect of the apex corner walls apparently well simulated. However, the viscous effects due to possible laminarization of the flow in the apex corner region cannot be represented with the present turbulent stress model and may well account for the observed discrepancies with measured axial velocity profiles.

The heat transfer calculations have shown that imposed boundary conditions have a significant effect on local and overall heat transfer and have suggested that the measured wall temperatures are probably more accurate than the heat fluxes. The results also confirm previous evidence that the hydraulic diameter concept is not valid for the prediction of friction and mean heat transfer in small apexed angled isosceles triangular ducts.

REFERENCES

1. C. W. Rapley, A summary of experimental turbulent non-circular passage flow and heat transfer, Report FS/80/41, Department of Mechanical Engineering, Imperial College, London (1980).
2. E. R. G. Eckert and T. F. Irvine, Flow in corners of passages with non-circular cross-sections, *Trans. Am. Soc. Mech. Engrs* **78,** 709 (1956).
3. E. R. G. Eckert and T. F. Irvine, Incompressible friction factors, transition and hydro-dynamic entrance length studies of ducts with triangular and rectangular cross-sections, *Proc. 5th Mid-west Conf. in Fluid Mech.*, p. 122 (1957).
4. L. W. Carlson and T. F. Irvine, Fully developed pressure drop in triangular shaped ducts, *Trans. Am. Soc. Mech. Engrs*, Series C, *J. Heat Transfer* 60-WA-100 (1961).
5. C. J. Cremers and E. R. G. Eckert, Hot wire measurements of turbulence correlations in a triangular duct, *Trans. Am. Soc. Mech. Engrs*, Series E, *J. Appl. Mech.* **29,** 609 (1962).
6. A. A. M. Aly, A. C. Trupp and A. D. Gerrard, Measurement and prediction of fully developed flow in an equilateral triangular duct, *J. Fluid Mech.* **85,** 57 (1978).
7. J. Nikuradse, Untersuchungen über turbulente strömungen in nicht kreisförmigen rohren, *Ing.-Arch.* **1,** 306 (1930).
8. E. R. G. Eckert and T. F. Irvine, Pressure drop and heat transfer in a duct with triangular cross-section, *Trans. Am. Soc. Mech. Engrs*, Series C, *J. Heat Transfer* **82,** 125 (1960).
9. B. E. Launder and W. M. Ying, Prediction of flow and heat transfer in ducts of square cross-section, *Proc. Instn Mech. Engrs* **187,** 455 (1973).
10. D. Naot, A. Shavit and M. Wolfshtein, Numerical calculation of Reynolds stresses in a square duct with secondary flow, *Wärme- und Stoffubertragung* **7,** 151 (1974).
11. P. Carajilescov and N. E. Todreas, Experimental and analytical study of axial turbulent flows in an interior subchannel of a bare rod bundle, *Trans. Am. Soc. Mech. Engrs*, Series C, *J. Heat Transfer* **98,** 262 (1976).
12. A. C. Trupp and A. M. M. Aly, Predicted secondary flows in triangular array rod bundles, *Trans. Am. Soc. Mech. Engrs, J. Fluids Engng* **101,** 354 (1979).
13. J. G. Bartzis and N. E. Todreas, Turbulence modelling of axial flow in a bare rod bundle, *Trans. Am. Soc. Mech. Engrs*, Series C, *J. Heat Transfer* **101,** 628 (1979).
14. A. D. Gosman, W. M. Pun, W. K. Runchal, D. B. Spalding and M. Wolfshtein, *Heat and Mass Transfer in Recirculating Flows*. Academic Press, New York (1969).
15. N. I. Buleev, Theoretical model of the mechanism of turbulent exchange in fluid flows, *A.E.R.E. Transl.* 957 (1963).
16. V. P. Bobkov, M. Ch. Ibragimov and G. I. Sabelev, Generalisation of experimental data on the intensity of velocity pulsations in turbulent flow of liquid in channels of various cross-sections, *Izv. Akad. Mech. Liquids Gases* No. 3, 162 (1968).
17. A. Tahir and J. T. Rogers, The mechanism of secondary flows in turbulent interchange in rod bundles, *Proc. 7th Canadian Congress Appl. Mech.*, p. 773 (1979).
18. A. F. Emery, P. K. Neighbors and F. B. Gessner, The numerical prediction of developing turbulent flow and heat transfer in a square duct, *Trans. Am. Soc. Mech. Engrs*, Series C, *J. Heat Transfer* **102,** 51 (1980).
19. A. D. Gosman and C. W. Rapley, Fully developed flow in passages of arbitrary cross-section, in *Recent Advances in*

Numerical Methods in Fluids (edited by C. Taylor and K. Morgan), Ch. 7. Pineridge Press, Swansea (1980).
20. W. J. Seale, Turbulent diffusion of heat between connected flow passages, Part 2, *Nucl. Engng Des.* **54,** 197 (1979).
21. A. D. Gosman and C. W. Rapley, A prediction method for fully developed flow through non-circular passages, *Proc. Int. Conf. Num. Meth. Lam. and Turb. Flow*, Swansea, p. 271 (1978).
22. C. W. Rapley, Fluid and heat flow in tubes of arbitrary cross-section, Ph.D. thesis, University of London (1980).
23. F. B. Gessner and A. F. Emery, A Reynolds stress model for turbulent corner flows, Part 1, *Trans. Am. Soc. Mech. Engrs, J. Fluids Engng* **92,** 261 (1976).
24. S. B. Pope, The calculation of turbulent recirculating flows in general orthogonal co-ordinates, *J. Comp. Phys.* **26,** 197 (1978).
25. B. L. Launder and D. B. Spalding, The numerical computation of turbulent flows, *Comp. Meth. Appl. Mech. Engng* **3,** 369 (1974).
26. B. E. Launder and D. B. Spalding, *Mathematical Models of Turbulence*. Academic Press, New York (1972).
27. L. S. Caretto, A. D. Gosman, S. V. Patankar and D. B. Spalding, Two calculation procedures for steady three-dimensional flows with recirculation, *Proc. 3rd Int. Conf. Num. Methods in Fluid Mech.*, Paris, p. 60 (1972).
28. R. C. Cope and R. W. Hanks, Transitional flow in isosceles triangles, *Ind. Engng Chem. Fund.* **11,** 106 (1972).
29. P. C. Bandopadhayay and J. B. Hinwood, On the co-existence of laminar and turbulent flow in a narrow triangular duct, *J. Fluid Mech.* **59,** 775 (1973).
30. W. M. Kays, *Convective Heat and Mass Transfer*, McGraw Hill, New York (1966).
31. E. M. Sparrow, Laminar flow in isosceles-triangular ducts, *A.I.Ch.E. Jl* **8,** 599 (1962).

APPENDIX

The constants in the ASTM [equations (10)–(15)] are related as follows [9, 23]:

$$C_1 = (22C_{\phi 1} - 24C_{\phi 2} + 8)/33(C_{\phi 1} - 2C_{\phi 2}),$$

$$C_2 = (12C_{\phi 1} - 4)/11(C_{\phi 1} - 2C_{\phi 2}),$$

$$C_3 = (22C_{\phi 1} - 36C_{\phi 2} - 10)/33(C_{\phi 1} - 2C_{\phi 2}),$$

$$C_4 = (44C_{\phi 1} - 22C_{\phi 1}C_{\phi 2} - 128C_{\phi 2} - 36C_{\phi 2}^2 + 10)/165(C_{\phi 1} - 2C_{\phi 2})^2,$$

where $C_{\phi 1}$ and $C_{\phi 2}$ are empirical coefficients.

LE CALCUL DE L'ECOULEMENT TURBULENT ET DU TRANSFERT THERMIQUE DANS UN CANAL TRIANGULAIRE ISOCELE ETROIT

Résumé—On décrit le calcul de l'écoulement turbulent établi et le transfert thermique dans un canal triangulaire isocèle étroit, à partir d'un organigramme dans lequel les contraintes de Reynolds sont calculées à partir des formes algébriques de leurs équations de transport, tout d'abord dérivées des calculs dans un canal carré. Les équations de base sont formulées dans un système de coordonnées orthogonales curvilinéaires qui est adapté à la forme de la section droite du canal. et elles sont résolues par une méthode efficace de volumes finies. Les solutions présentées montrent que, pour le canal à faible angle au sommet, la convection thermique locale ou moyenne n'est pas sensiblement affectée par l'écoulement secondaire, tandis qu'elle est sensible aux conditions de température imposées aux limites. Les calculs se comparent favorablement avec les expériences et ils sont utiles pour leur interprétation.

BERECHNUNG DER TURBULENTEN STRÖMUNG UND WÄRMEÜBERTRAGUNG IN EINEM ENGEN, GLEICHSCHENKLIGEN DREIECKSKANAL

Zusammenfassung—Die Berechnung der voll ausgebildeten turbulenten Strömung mit Wärmeübertragung in einem engen, gleichschenkligen Dreieckskanal wird beschrieben. Sie wurde durchgeführt mit Hilfe eines Rechenmodells, in welchem die Reynoldsschen Spannungen aus algebraischen Formen ihrer Transportgleichungen berechnet werden, und welches zuerst für Rechnungen im Zusammenhang mit einem Rechteckkanal hergeleitet wurde. Die Bestimmungsgleichungen werden in einem orthogonalen krummlinigen Koordinatensystem aufgestellt, welches der Form des Kanalquerschnitts angepaßt wird, und durch eine leistungsfähige finite Volumenmethode gelöst. Die vorgelegten Ergebnisse zeigen, daß für die Bedingungen des untersuchten Kanals mit einem kleinen Scheitelwinkel die örtlichen und mittleren Wärmeübergangskoeffizienten relativ wenig durch die Sekundärströmung beeinflußt werden, während sie ziemlich empfindlich gegenüber der angenommenen Randbedingung für die Temperatur sind. Die vorgelegten Rechenergebnisse stimmen gut mit den Experimenten überein und erweisen sich als brauchbar für deren Interpretation.

РАСЧЕТ ТУРБУЛЕНТНОГО ТЕЧЕНИЯ И ТЕПЛОПЕРЕНОСА В УЗКОМ КАНАЛЕ С СЕЧЕНИЕМ В ФОРМЕ РАВНОБЕДРЕННОГО ТРЕУГОЛЬНИКА

Аннотация—Описаны расчеты полностью развитого турбулентного течения и теплопереноса в узком канале с сечением в форме равнобедренного треугольника, полученные с помощью модели, для которой напряжения Рейнольдса определяются из решения алгебраических уравнений переноса, первоначально предложенных для каналов квадратного сечения. Основные уравнения формулируются в системе ортогональных криволинейных координат, соответствующих форме поперечного сечения канала, и решаются эффективным методом конечного объема. Полученные решения показывают, что для исследуемого канала с небольшим углом у вершины локальный и суммарный теплоперенос почти не зависят от вторичных течений, но зависят от налагаемых температурных граничных условий. Показано, что результаты расчетов удовлетворительно согласуются с экспериментальными данными и могут использоваться для их обобщения.